Draft June 7th 2015

The role of steric effects and acidity effects in direct synthesis of iso-paraffins from syngas on cobalt zeolite catalysts

Vijayanand Subramanian[a], Vladimir Zholobenko[b], Kang Cheng[c], Christine Lancelot[a], Sébastien Paul[a], Vitaly V. Ordomsky[a]*, Andrei Y. Khodakov[a]*

[a] *Unité de catalyse et de chimie du solide (UMR 8181 CNRS), Université Lille 1-ENSCL-EC Lille, Bat. C3, Cité Scientifique, 59655 Villeneuve d'Ascq, France*

[b]*School of Chemistry and Physics, Keele University, Staffordshire, ST5 5BG, United Kingdom*

[c]*State Key Laboratory of Physical Chemistry of Solid Surfaces, College of Chemistry and Chemical Engineering, Xiamen University, Xiamen 361005, China*

Corresponding authors: vitaly.ordomsky@univ-lille1.fr (V.V. Ordomsky), andrei.khodakov@univ-lille1.fr (A.Y. Khodakov)

Abstract

The paper focuses on the effects of localization of cobalt species, zeolite structure and acidity on the performance of cobalt bifunctional catalysts promoted with platinum for direct synthesis of iso-paraffins from syngas. ZSM-5, MOR and BEA have been chosen as zeolites with different structure and pore diameter. The catalysts were prepared either by incipient wetness impregnation or mechanical mixing of zeolite with a conventional silica supported cobalt Fischer-Tropsch catalyst. Low temperature nitrogen adsorption, scanning and transmission electron microscopy, temperature programmed reduction and infra-red spectroscopy with adsorbed molecular probes were used for catalyst characterisation.

The increase in the size and the open character of the zeolite pore structure from ZSM-5 to BEA resulted in a higher fraction of cobalt located inside the pores of the catalysts prepared by impregnation. The catalytic performance was strongly affected by the zeolite acidity, pore structure and cobalt distribution between the zeolite pores and external surface. The selectivity to short chain iso-paraffins is principally affected by the zeolite acidity, while the selectivity to long chain branched hydrocarbons mostly depends on the steric effects such as zeolite pore sizes and cobalt partition between the zeolite pores and outer surface. The impregnated catalysts showed significantly higher selectivity to long-chain iso-paraffins in comparison with mechanically mixed hybrid catalysts. The effect was more pronounced for the three-dimensional large-pore BEA zeolite prepared by impregnation with higher fraction of cobalt inside the zeolite pores.

Keywords: syngas; Fischer-Tropsch synthesis; gasoline; iso-paraffins; zeolites

1. Introduction

Ultra-clean liquid fuels can be produced from alternatives to petroleum sources like natural gas, biomass and coal through intermediate transformation into syngas ($CO+H_2$) and subsequent Fischer-Tropsch synthesis (FT) over iron or cobalt based catalysts [1, 2, 3]. Low temperature FT synthesis over cobalt containing catalyst is very attractive because of the high cobalt intrinsic activity, higher conversion per single cycle and better catalyst stability compared to iron catalysts [2]. FT synthesis is a "non-trivial surface polymerization reaction" [4], which exhibits a broad distribution of the linear hydrocarbons; the reaction selectivity is typically described using the Anderson-Schulz-Flory (ASF) distribution model [5, 6]. Directing the reaction selectivity to specific hydrocarbon fractions is therefore a main challenge of FT synthesis.

Several methods were proposed to control the selectivity of this reaction. FT synthesis can be combined with hydrocracking and isomerization of long–chain hydrocarbons in order to restrict hydrocarbon distribution to a specific range. Isomerization and cracking of FT hydrocarbons would lead to iso-paraffins or diesel fuels constituted by C_{10}-C_{20} hydrocarbons. A possible option to produce these fuels directly from syngas would be to use hybrid or composite catalysts containing both an active FT component (Co, Fe or Ru catalyst) and an acid catalyst active in cracking and isomerization.

Owing to their high acidity and stability, zeolite and metal/zeolite materials have been proposed as some of the most efficient catalysts for hydrocarbon cracking and isomerization under the conditions close to FT synthesis [3, 7]. An FT catalyst can be integrated with a zeolite or metal/zeolite in several different ways: (1) in the dual-bed configuration of the catalytic reactor with the FT catalyst in the first layer and the zeolite or metal/zeolite in the second [8, 9]; (2) as core-shell catalysts [10 , 11 , 12, 13]; (3) as hybrid catalysts prepared by

mechanical mixing the FT catalyst with the zeolite [14, 15]; (4) by the introduction of the FT active metal into the zeolite via impregnation [16, 17, 18].

The dual-bed systems are likely to demonstrate low efficiency for direct iso-paraffins synthesis because of the high volume and difficult process control. Synthesis of core-shell catalysts requires rather sophisticated preparation methods [13]. A number of publications have addressed direct synthesis of gasoline over hybrid catalysts prepared by mechanical mixing of supported cobalt catalysts with zeolites [19, 20, 21, 22, 23]. Different types of zeolites such as ZSM-5, MCM-22, IM-5, ITQ-2, BEA, MOR and Y with and without noble metal promoters have been used for the preparation of such hybrid catalysts. A high ratio of iso- to linear paraffins (C_{iso}/C_n) has been observed over hybrid catalyst containing Co/SiO_2 and Pd/BEA or Pd/Y [23]. At the same time, slow diffusion of long-chain paraffins through the pores of 10-membered ring zeolites, such as ZSM-5, leads to preferential participation of the external surface acid sites resulting in a lower efficiency of isomerization [19].

Impregnation is another way for the preparation of bifunctional cobalt zeolite catalysts [16, 17, 18, 24, 25, 26]. A major drawback of this procedure, however, could be neutralization of the zeolite acid sites by the introduced cobalt cations. This could result in a simultaneous decrease in the number of acidic sites available for hydrocarbon cracking and isomerization and in the extent of cobalt reduction as isolated cobalt ions in the zeolite cationic sites are very difficult to reduce to metallic cobalt. The choice of the best preparation method for bifunctional catalysts for the direct synthesis of iso-paraffins from syngas would depend on the zeolite acidity and its porous structure.

The main aim of this work is to elucidate the structural effects such as localization of cobalt species, zeolite pore structure and zeolite acidity on the properties of cobalt zeolite bi-functional catalysts and their catalytic performance for the direct iso-paraffins synthesis from syngas. Zeolites with different porous structure, i.e. ZSM-5, mordenite (MOR) and beta-

zeolite (BEA), have been used in this work. The catalysts have been characterized using low temperature nitrogen adsorption, transmission and scanning electron microscopy (TEM and SEM), temperature programmed reduction (TPR) and infra-red spectroscopy with adsorbed pyridine and carbon monoxide. The catalytic performance has been evaluated in a Flowrence high-throughput system (Avantium®) equipped with 16 parallel fixed-bed milli-reactors.

2. Experimental

2.1. Catalyst preparation

Commercial amorphous silica (CARIACT Q-10, Fuji Silysia) was used for the preparation of a conventional silica supported FT catalyst. The silica supported catalyst (20 wt. % Co and 0.1 wt. % Pt) was prepared by incipient wetness impregnation using aqueous solutions of cobalt nitrate ($Co(NO_3)_2 \cdot 6H_2O$, suppliers for all chemicals?) and tetramine platinum nitrate ($[Pt(NH_3)_4](NO_3)_2$). The ZSM-5, MOR and BEA zeolites with the Si/Al ratio of 13, 8 and 9, respectively, were provided by Zeolyst.

The Co-containing zeolite were prepared by incipient wetness impregnation of zeolite with cobalt nitrate ($Co(NO_3)_2\ 6H_2O$) and tetramine platinum nitrate ($[Pt(NH_3)_4])NO_3)_2$). The Co and Pt content was 20 and 0.1 wt. %, respectively. The prepared catalysts were calcined in air at 450°C. The hybrid catalysts were prepared by mechanical mixing of different zeolites with the silica supported catalyst. The ratio of zeolite to Co in the mechanical mixture was (4:1 wt., i.e. the same as in the impregnated catalysts). For the catalytic tests, the cobalt and platinum weight loadings by mass in the reactor were exactly the same in the impregnated samples and in hybrid catalysts prepared using mechanical mixing.

2.2. Characterization

The BET surface area, pore volume and average pore diameter were determined by N_2 low temperature adsorption using a Micromeritics ASAP 2000 automated system. The samples were degassed under vacuum at <10 μm Hg at 300°C for 4 h prior to N_2 physisorption. The total pore volume (TPV) was calculated from the amount of vapor adsorbed at a relative pressure close to unity assuming that the pores are filled with the condensate in liquid state. The catalyst external surface area and micropore volume were calculated using deBoer t-plot method [27].

The electron micrographs were obtained by MIRA-LMH (Tescan) scanning electron microscope (SEM) equiped with a field emission gun. The TEM observations of the samples were performed on a Tecnai instrument, equipped with a LaB6 crystal, operating at 200 kV. Prior to the analysis, the samples were dispersed by ultrasound in ethanol for 5 min, and a drop of the suspension was deposited onto a carbon membrane on a 300 mesh-copper grid.

The catalyst reducibility was studied using a temperature-programmed reduction (TPR). system equipped with a TCD detector. The samples were reduced in a flow of 5 % H_2/Ar (60 ml/min) and heated up to 900 °C at a rate of 10 °C/min.

The IR spectra were recorded with a Nicolet Protégé 460 FT-IR spectrometer at 4 cm^{-1} resolution. Prior to the measurements, the catalysts pressed in self-supporting discs (~10mg/cm^2) were activated in the IR cell attached to a vacuum line at 400°C for 4 h. The catalysts were reduced in the atmosphere of H_2 at 400°C with subsequent evacuation. Adsorption of CO over the impregnated catalysts has been carried out at room temperature (P_{CO} was varied from 0 to 20 torr). Adsorption of pyridine (Py) was performed at 150°C for 10 minutes. The excess of probe molecules was evacuated at the same temperature for 30 minutes. The evacuation was repeated in a stepwise fashion every 50°C up to 450°C.

2.3. Catalytic tests

Carbon monoxide hydrogenation was carried out on the REALCAT platform in a Flowrence high-throughput system (Avantium®) [28] equipped with 16 parallel fixed-bed milli-reactors (d=2 mm) with a plug-flow hydrodynamics operating at a total pressure of 20 bar, 250°C, H_2/CO= 2 molar ratio and GHSV of 34 L/g_{Co} h. The catalyst loading was 50 mg per reactor in the case of impregnated catalysts. In the case of hybrid catalysts, the same amount of cobalt and zeolite (by mass) was placed in the reactor which corresponded to 90 mg of the catalyst. Prior to the catalytic tests, all the samples were activated in a flow of H_2 at atmospheric pressure for 10 h at 400°C. During the activation step, the temperature ramp was 3°C/min. After the activation, the catalysts were cooled down to 180°C and a flow of premixed syngas was gradually introduced into the reactor. When the pressure attained 20 bar, the temperature was slowly increased to 250°C. The gaseous reaction products were analyzed by on-line gas chromatography. Analysis of permanent gases was performed using a Molecular Sieve column and a thermal conductivity detector. Carbon dioxide and C_1-C_4 hydrocarbons were separated on a PPQ column and analyzed by a thermal conductivity detector. The C_5-C_{12} hydrocarbons were analyzed using a CP-Sil5 column and a flame-ionization detector. High-molecular-weight products were collected at atmospheric pressure in vials heated at 60°C. Carbon monoxide contained 5% of helium, which was used as an internal standard for calculating the carbon monoxide conversion. The reaction rates were defined as the number of moles of CO converted per hour per gram of the catalyst or cobalt(?) (mol/g·h). The product selectivity (S) was reported on carbon atom basis.

3. Results and discussion

3.1. Characterization

The N_2 adsorption–desorption isotherms for the catalysts prepared by impregnation as compared to those for the parent zeolites are shown in Figure 1. The ZSM-5 and MOR

samples display Type-I isotherms, which exhibit a sharp uptake at low relative pressure followed by plateau without a hysteresis. This type of isotherm is usually observed for microporous materials. The BEA zeolite exhibits a combination of Type I and IV isotherms, which shows a high N_2 uptake at low relative pressure and a hysteresis loop at high relative pressure ($p/p_o > 0.8$). Adsorption of nitrogen in the range of $p/p_0 = 0.8 - 1.0$ can be explained by filling of the inter-crystalline pores [29]. The amorphous silica support demonstrates mainly N_2 adsorption at high pressures due to the filling of silica inter-particle spaces. The SEM micrographs of the ZSM-5, MOR and BEA zeolites (Figure 2) display agglomerates of relatively small crystallites (< 100 nm).

Impregnation with cobalt and platinum does not lead to any significant changes in the nitrogen adsorption isotherms over ZSM-5, MOR and silica support. Impregnation of the BEA zeolite leads to the disappearance of the high pressure hysteresis loop and the appearance of a new sharp step in the isotherm at $p/p_0 \approx 0.2$. This is probably related to the rearrangement of small zeolite crystallites in the agglomerates of the impregnated BEA sample.

The textural properties are presented in Table 1. A significant decrease in the zeolite surface area and pore volume is observed after impregnation with cobalt and platinum. The decrease in surface area and pore volume after the impregnation is more significant in BEA (~50 %), followed by MOR zeolite (~25 %) and ZSM-5 (17%). Note that the surface area and pore volume of Co/ZSM-5 only slightly decrease relative to the parent zeolite. The difference between the surface area of Co/ZSM-5 and Co/MOR and their parent zeolites may be assigned to the effect of zeolite “dilution” in the impregnated catalyst due to the presence of 20 wt. % of cobalt. The three-dimensional pore structure of BEA (0.76×0.64 nm) is more open that of MOR (0.65×0.7 nm; uni-dimensional) and ZSM-5 (~0.55 nm; three-dimensional). A more significant decrease in the BET surface area and micropore volume of BEA as

compared to ZSM-5 and MOR zeolites could be assigned therefore to a much easier diffusion of cobalt species into zeolite pores during the impregnation leading to a higher cobalt fraction in the pores of BEA.

In order to further confirm the influence of the zeolite pore size on cobalt distribution between the zeolite pores and external surface, the impregnated catalysts have been analyzed by transmission electron microscopy (see Figure 3). In agreement with previous data [30], the TEM images of the reference Co/SiO_2 demonstrates irregularly distributed Co nanoparticles with the diameter in the range 10-50 nm. In the impregnated calcined Co/ZSM-5, polycrystalline zeolite particles are covered by large agglomerates of cobalt nanoparticles (100-200 nm). The metal does not seem to be present inside of the zeolite pores. The results are consistent with the preferential cobalt localization on the external surface of the ZSM-5 zeolite. The TEM images of Co/MOR demonstrate a significantly higher incorporation of Co in the zeolite crystallites, although some fraction of cobalt nanoparticles can be observed on the surface of zeolite crystals. The TEM images of Co/BEA show that the zeolite crystallites are almost totally dark colored by cobalt which is located inside of the zeolite crystals. This is consistent the cobalt localization inside the zeolite pores could also explain a significant decrease in the surface area and pore volume of zeolite BEA after the impregnation.

The TPR profiles of the reference catalyst and zeolites are shown in the Figure 4. The TPR curve of the reference Co/SiO_2 catalyst exhibits two groups of peaks at 200 and 400°C. In agreement with the previous reports [31, 32], the first peak can be assigned to the reduction of Co_3O_4 to CoO. The second peak at 400°C is mainlydue to the reduction of CoO to metallic Co. Note that TPR profiles of the impregnated cobalt zeolite catalysts display only a single group of peaks around 350-400°C. The TPR profiles of the cobalt containing zeolites are consistent with previous results [33, 34, 35, 36] and could be attributed to the reduction of small CoO_x species located either on the external surface or inside of the zeolite pores. The

position of these peaks depends on the zeolite structure. The principal peaks in the TPR profiles of Co/BEA and Co/MOR samples are located at lower temperatures than in Co/ZSM-5, which would leads to a higher fraction of metallic cobalt in the reduced Co/BEA and Co/MOR catalysts. Note that the Co/ZSM-5 zeolite also exhibits a small peak at 600° C that can be assigned to the reduction of smaller cobalt oxide particles located in the narrower pores of this zeolite. The peaks attributed to the reduction of Co^{2+} ions in the zeolite cationic positions have not been observed; this would take place above 800^{o}C, as has been shown previously [33, 34, 35, 36].

The acid and metal sites in the initial and Co containing reduced samples have been studied by FTIR spectroscopy. Several bands have been distinguished in the spectrum of samples in the region of OH- stretching vibrations (Figure 5). The band observed at 3743 cm^{-1} is attributed to the external silanol groups. This band has the highest intensity in silica and in BEA zeolite. The band at 3735 cm^{-1} is observed only in zeolite BEA and is usually attributed to the internal silanol groups. The bands at 3610 and 3664 cm^{-1} are due to the bridged acid hydroxyl groups (Si-(OH)-Al) and extraframework AlOH species, respectively. The 3610 cm^{-1} band has a significantly higher intensity in MOR and ZSM-5 as compared to the BEA zeolite. The band at 3782 cm^{-1} is observed only in BEA, it can be assigned to hydroxyl groups attached to three-coordinated Al atoms, similar to those in alumina [37, 38].

Thus, the spectra of zeolite BEA indicate the presence of a considerable number of defect sites. Indeed, it has been shown that the BEA structure can be readily dealuminated during calcination with deposition of extraframework aluminum species inside the channels [39, 40].

Impregnation with cobalt does not significantly affect the spectra of the silica supported catalyst. Only a slight decrease in the intensity of silanol groups is observed. In contrast, impregnation of the zeolites with cobalt leads to a major decrease in the intensity of IR bands

attributed to the bridged hydroxyls, silanols and extraframework AlOH groups. These bands almost completely disappear in the spectra of the Co/BEA catalyst, indicating a higher cobalt dispersion in this zeolite and a significant cobalt incorporation inside the zeolite pores as well as a high coverage of the external surface of BEA by cobalt species. The effect of impregnation on the intensity of OH groups is less pronounced for MOR and ZSM-5 samples. Indeed, a moderate decrease in the intensity of the bridged OH groups in the ZSM-5 zeolite after the impregnation is consistent with a smaller fraction of cobalt species located inside the pores of these zeolites. These results are in good agreement with the nitrogen adsorption and TEM data (Figures 3 and 4), which suggest preferential cobalt localization on the external surface of ZSM-5.

The IR spectra recorded after Py adsorption on the reduced catalysts are presented in Figure 6. No IR bands attributed to adsorbed Py have been observed on the Co/SiO_2 catalyst. This indicates the absence of both Brønsted (or Broensted but not Brönsted) and Lewis acid sites (BAS and LAS) in this catalyst. With the zeolite catalysts, the chemisorbed pyridine exhibits characteristic bands at 1545 cm^{-1} assigned to pyridinum ion (PyH^+) and ~1450 cm^{-1} assigned to Py adsorbed on LAS (which may include Co^{2+} ions). (Please note the correct assignment, the band at 1615-1625 cm^{-1} is due to Py adsorbed on LAS, and the band at 1635-1640 cm^{-1} is due to pyridinum ion, PyH^+.) Py adsorbed on both LAS an BAS displays also a band at 1490 cm^{-1}. The effective strength of Brønsted acid sites has been evaluated from the variation of the band intensity at 1545 cm^{-1} as a function of Py desorption temperature. Figure 7 shows that Py desorption proceeds more easily from BAS of BEA compared to MOR and ZSM-5 zeolites. The MOR and ZSM-5 zeolites demonstrate similar effective strength of acid sites with a slightly higher desorption temperature for MOR. These results are in line with previous ammonia TPD data for the same zeolites [41].

The concentration of BAS and LAS calculated using published extinction coefficients for the bands at 1545 cm^{-1} and 1450 cm^{-1} [42] are presented in Table 1. The results suggest that impregnation with cobalt and platinum leads to a significant decrease in the concentration of BAS in the zeolites. The effect is more pronounced for the BEA zeolite compared to MOR and ZSM-5. Indeed, Co/ZSM-5 retains about 50 % of Brønsted acidity after impregnation, while the concentration of BAS in Co/BEA is only 18 % compared to the parent zeolite. In contrast, a reversed order is observed for pyridine adsorption on LAS in the impregnated reduced catalysts. The number of LAS in ZSM-5 significantly increases in the presence of cobalt and platinum in comparison with the parent sample. The effect is smaller in the case of the MOR zeolite. At the same time, the parent BEA zeolite already demonstrates significant Lewis acidity due to its defect-rich structure in comparison with ZSM-5 and MOR. Impregnation with cobalt leads to almost complete removal of Py-LAS band from the spectrum of Co/BEA.

The decrease in the number of BAS in Co/ZSM-5, Co/MOR and Co/BEA relative to the parent zeolites, can be accounted for by the ion exchange of the bridging OH-group protons for Co^{2+} ions and by partial removal of the Al-OH groups. Both the ion exchange and the presence of incompletely reduced CoO_x species could explain the significant increase in Lewis acidity over Co/ZSM-5, as Py can interact with cationic cobalt species. The weak or negative effect of Co introduction on Lewis acidity in BEA and MOR may be due to a more complete Co reduction in these zeolites, as confirmed by TPR. Furthermore, the presence of a significant amount of Co inside the large pore BEA and MOR (possibly in metallic state) may result in the pore blocking, hindering Py access to the LAS. Indeed, nitrogen adsorption and TEM data suggest a much higher cobalt concentration inside the pores of BEA and MOR.

Figure 8 shows spectra of CO adsorbed on the Co/SiO_2 catalyst and the impregnated zeolites. The catalysts exhibit two IR bands at 2190-2205 and 2060-2070 cm^{-1} attributed to

CO adsorbed species. The bands in the region of 2200-2205 cm^{-1} can be assigned to CO adsorption on cobalt cations (there are no Lewis sites in this sample, also the stability of this band suggests it cannot be due CO adsorption on LAS) [43, 44]. This band has low intensity in the reference Co/SiO_2 and is shifted to lower frequencies in comparison with the zeolite based catalysts. In agreement with previous data [44], in the Co/SiO_2 catalyst this band results from CO adsorption on cobalt cations in amorphous cobalt silicates. In the case of Co/ZSM-5 and Co/MOR, the intensity of the band at 2205 cm^{-1} is high due to CO adsorption over a large number of cationic cobalt sites inside the zeolite pores. The intensity of this band is significantly lower for Co/BEA. These results complement our Py adsorption data, which show a higher concentration of unreduced cations in ZSM-5 in comparison with MOR and BEA.

The bands below 2100 cm^{-1} can be attributed to CO adsorbed on reduced Co^0. The CO bands in the region of 2050-2070 cm^{-1} show an ~10 cm^{-1} blue-shift for Co/Zeolite samples as compared to CO--Co^0 sites in the silica supported catalyst [44, 45]. This is probably due to the smaller particle size and the positive charge on the cobalt metal nanoparticles induced by their interaction with the zeolite BAS [46]. The spectrum of Co/BEA catalyst shows an additional band at 1887 cm^{-1} which can be assigned to the bridged adsorption of CO on Co^0 sites. This low frequency band is indicative of higher fraction of smaller Co metallic nanoparticles which could be located inside of the BEA zeolite pores.??? The band of CO adsorbed on metallic Co sites exhibits the highest intensity over Co/ZSM-5, which can be explained by CO adsorption on highly dispersed Co on the ZSM-5 external surface.

Thus, characterization of the impregnated Co-zeolite catalysts using IR spectroscopy, electron microscopy and sorption-desorption measurements suggests a significant influence of the zeolite porous structure on the cobalt distribution between the external and internal surface of the zeolite and itsreducibility. Cobalt species in the BEA zeolite are more easily

reduced compared to MOR and ZSM-5 showing a higher fraction of reduced cobalt present inside the more open pore structure of BEA zeolite. In addition, a higher concentration of stronger acid sites is found in Co/ZSM-5 catalyst compared to Co/MOR and Co/BEA.

3.2. Catalytic performance in FT synthesis

3.2.1. Catalytic activity

The results of catalytic tests for the studied cobalt catalysts, measured in a high throughput Flowrence fixed-bed mill-ireactor system, are presented in Table 2 and Figures 9-12. Hydrocarbons and water have been the major reaction products, whereas the CO_2 selectivity has always been lower than 2%. The reference Co/SiO_2 catalyst exhibited stable activity during 40 h with conversion of about 40 % (Figure 9).

The catalysts prepared by ion exchange of the zeolites with cobalt nitrate did not show any measurable activity in FT synthesis (not shown). Indeed, FT synthesis occurs on cobalt metal sites. The cationic metal sites present in the ion exchange positions of zeolites cannot be reduced under the reaction conditions and do not participate in the FT synthesis.

The catalytic performance of the samples prepared either by impregnation or mechanical mixing is strongly affected by the zeolite used and the preparation method. FT synthesis is a complex reaction and the reaction rate could be affected by the number and intrinsic activity of cobalt active sites, zeolite acidity, reagent and product diffusion. Note that in this work, FT synthesis on Co-catalysts exhibits different selectivity especially towards the long-chain hydrocarbons (C_{20+}) as discussed further in greater details.

The hybrid catalysts prepared by mechanical mixing of Co/SiO_2 with zeolites display different activity in comparison with the reference catalyst. The carbon monoxide conversion on Co/SiO_2+ZSM-5 is lower in comparison with the reference Co/SiO_2 catalyst. The conversion over Co/SiO_2+MOR is similar to the reference catalyst, while the Co/SiO_2+BEA

catalyst shows a significantly higher activity than the reference Co/SiO_2. Interestingly, the catalysts prepared by impregnation of the ZSM-5 and MOR zeolites demonstrate activity similar to their counterparts prepared by mechanical mixing. This can be explained by the preferential location of cobalt in these impregnated catalysts mainly on the surface of zeolite crystals and a low cobalt content inside the zeolite pores. The Co/BEA zeolite prepared by impregnation shows a lower FT reaction rate compared to the hybrid catalyst prepared by mechanical mixing. The catalytic results are consistent with CO adsorption data. Low CO adsorption on metallic Co species in BEA zeolite could explain low activity of the catalyst (Figure 8). Significantly higher deactivation rates over impregnated Co/BEA and Co/MOR have been observed in comparison with the hybrid catalysts, while the catalytic performance of Co/ZSM-5 catalyst has been relatively stable.

3.2.2. Hydrocarbon selectivities

Table 2 shows the hydrocarbon distribution on the hybrid catalysts prepared by mechanical mixing and on the impregnated samples. The selectivity to methane is about 6 % over the reference and hybrid catalysts. In comparison with the reference and hybrid catalysts, the impregnated catalysts exhibite almost two times higher selectivity to methane. In contrast, to the hybrid samples, the impregnated catalysts contain some amount of cobalt metallic sites inside the zeolite [47]. On one hand, slow diffusion of long chain hydrocarbons inside of zeolite pores and their interaction with metal particles located inside the zeolites would lead to hydrocarbon secondary hydrocracking and increase methane production. On other hand, Iglesia et al [48, 49] have shown that diffusion limitations in the catalyst pores could be higher for carbon monoxide in comparison with hydrogen. This would lead to higher effective H_2/CO ratio in the catalyst pores and respectively to higher selectivity to methane and lighter hydrocarbons.

Mostly linear hydrocarbons and very small amounts of iso-paraffins have been observed over the Co/SiO_2 reference catalyst (Figure 10, Table 2). This is consistent with previous reports [2, 4, 48, 49] and could be attributed to the absence of strong acid sites in the silica support (see Figure 5), which would initiate the formation of carbocations with subsequent skeletal isomerization, possible ß-scission and formation of short chain isomers [50]. In agreement with previous reports [48, 49], the olefin to paraffin ratio increases with increase in the hydrocarbon chain length (Figure 10). This fact could be due to the olefin secondary reactions in the Co/SiO_2 catalyst: hydrogenation and possible olefin insertion in the FT polymerization chain [48, 49]. The probability of olefin secondary hydrogenation reactions could be higher for long-chain hydrocarbons due to their slow diffusion in FT catalysts.

The hydrocarbon selectivity observed on both impregnated and hybrid cobalt-containing zeolite catalysts is dependent on the zeolite acidity, zeolite porous structure and catalyst preparation method. Indeed, the selectivity towards the lighter C_5-C_{12} hydrocarbons is much lower for both impregnated and hybrid cobalt-zeolite catalysts as compared to Co/SiO_2 (Table 2). This is probably due to higher olefin reactivity on the zeolite acid sites. The low olefin selectivity in the bifunctional cobalt-zeolite cataysts coincides with the presence of significant amounts of iso-paraffins in the reaction products. Previous studies [50] suggest that paraffin isomerization on the metal containing zeolites proceeds via intermediate formation of olefins. Our results show that light olefins, which are always present during FT synthesis over Co catalysts, might participate in the isomerization reaction. The isomerization however seems to also involve paraffins. Indeed, the amounts of produced isoparaffins are significantly higher than the amounts of olefins produced in conventional FT synthesis over the reference Co/SiO_2 catalyst. The ratio of isomers to the total amount of hydrocarbons in the C_5-C_{12} range increases from 0.3 to 0.7 in the following order for the catalysts prepared using either impregnation or mechanical mixing : BEA< MOR< ZSM-5. The reason for the higher

isomerization activity of MOR and ZSM-5 supported catalysts towards the short chain C_5-C_{12} hydrocarbons in comparison with BEA is the significantly higher number of strong BAS monitored in this work by Py adsorption (Figures 6 and 7).

The hybrid Co/SiO_2+ZSM-5 and impregnated Co/ZSM-5 catalysts show similar C_5-C_{12} olefin and paraffin selectivities (Table 2). In both samples, cobalt is largely located on the external surface of the zeolite crystals, hence, the zeolite acid sites are only slightly affected by cobalt species, and therefore, are available for isomerization of short chain hydrocarbons . The Co/MOR impregnated catalyst demonstrates a significantly lower activity in the isomerization of short-chain hydrocarbons compared to the relevant hybrid catalyst. This could be due to the partial blocking of strong acid sites by cobalt species in the uni-dimentional channels of the impregnated Co/MOR catalysts. Both impregnated and hybrid cobalt BEA catalysts exhibit low C_5-C_{12} hydrocarbon isomerization activity (Table 2). This should be attributed to the lower number of strong BAS in the BEA zeolite compared to ZSM-5 and MOR. It can be concluded that the rate of C_5-C_{12} hydrocarbon isomerization is principally affected by the number of the strong acid sites in the zeolite catalysts. No noticeable effect of the zeolite pore sizes on the C_5-C_{12} hydrocarbon isomerization activity has been detected.

Different selectivity results have been obtained for the C_{12+} hydrocarbons in comparison with the short-chain C_5-C_{12} paraffins. For the reference Co/SiO_2, hybrid and impregnated cobalt-zeolite catalysts, the distribution of long-chain hydrocarbons shows a maximum at about C_{20} (Figure 11). In the cobalt zeolite catalysts prepared by either mechanical mixing or impregnation, the distribution of C_{20+} hydrocarbons is rather different from that observed in the conventional Co/SiO_2 catalyst. The long-chain hydrocarbon selectivity is affected by both the zeolite structure and catalyst preparation procedure. Over the Co/SiO_2+ZSM-5 and Co/ZSM-5, the distribution of the C_{20+} normal hydrocarbons has similar shape and with the

similar chain growth probability (α=0.87) (Figure 12). The fraction of C_{20+} branched hydrocarbons is relatively small for both ZSM-5 based catalysts prepared by impregnation and mechanical mixing. Activity of these catalysts in the isomerization of longer C_{20+} hydrocarbons is relatively low, which can be explained by diffusional contains for the C_{20+} hydrocarbons in the zeolite pores. Our data indicate that cobalt species in Co/ZSM-5 and Co/SiO_2+ZSM-5 are mostly located on the zeolite external surface, suggesting that FT synthesis in these catalysts occurs on the zeolite external surface and that only short chain hydrocarbons can effectively diffuse and isomerize inside the pores of zeolite ZSM-5. Indeed, the catalysts prepared using ZSM-5 exhibit higher activity towards the isomerization of C_5-C_{12} hydrocarbons.

The fraction of C_{20+} long chain hydrocarbons is significantly lower in the MOR and BEA based zeolites (Table 2, Figure 11). The distribution of long chain hydrocarbons on both zeolites shows noticeable deviations from the standard ASF model (Figure 12). It appears that larger zeolite pore favor diffusion of long-chain hydrocarbons into the zeolite pores with their subsequent cracking. The most significant decrease in the fraction of long chain hydrocarbons is observed for the BEA based catalysts, which have the most open pore system among the investigated zeolites. The GC analysis is also consistent with visual aspects of the liquid samples produced over different catalysts. The wax produced over Co/BEA is liquid in comparison with solid wax formed over Co/ZSM-5 and Co/MOR samples (Figure 11). The fraction of the branched C_{12+} hydrocarbons is much more significant for the BEA and MOR based catalysts in comparison with ZSM-5 based counterparts, although ZSM-5 has a higher concentration of strong BAS compared to the BEA zeolite. For the long chain hydrocarbons, our selectivity results point to a more significant effect on the catalyst hydrocracking and isomerization activity resulting from the more open structure and larger pore size of BEA

rather than from its acidity. This is different for short chain hydrocarbons whose isomerization is mostly affected by the zeolite acidity.

The distribution of long chain hydrocarbons is also affected by the catalyst preparation method. The fraction of the C_{20+} hydrocarbons is much smaller in the catalysts prepared by impregnation compared to the hybrid mechanically mixed catalysts (Figure 11) This indicates a greater role of hydrocracking on the impregnated catalysts, which contain a higher fraction of cobalt species inside the zeolites crystallites, particularly for the large pore BEA and MOR. The close proximity between the cobalt metallic species located in the zeolite pores and the zeolite acid sites favors secondary reaction of long chain hydrocarbons, i.e. cracking and isomerization. In contrast, spatial effects on the selectivity towards short chane normal and iso-paraffins are less substantial owing to the relatively fast diffusion of the C_5-C_{12} hydrocarbons in the catalyst pores.

5. Conclusion

Sample characterization and catalytic results indicate strong influence of the zeolite pore structure and acidity on the formation of cobalt species and on the performance of cobalt-zeolite bifunctional catalysts in FT synthesis. In the catalysts prepared by impregnation, the distribution of cobalt species between the pores and the external surface of ZSM-5, MOR and BEA is strongly affected by the zeolite pore structure. Such cobalt species can be present in the zeolite pore in both metallic and cationic state. A greater fraction of cobalt is located inside the large-pore MOR and BEA zeolites. Cobalt can be more easily reduced in the pores of BEA and MOR compared to ZSM-5.

The catalytic performance in FT synthesis appears to be a function of the cobalt distribution between the zeolite pores and the outer surface, cobalt reducibility, zeolite pore structure and acidity. In particular, the rate of hydrocracking and isomerization of

hydrocarbons is dependent on both the zeolite acidity and its pore structure. Different zeolite characteristics have an effect on hydrocarbon selectivity for short and long chain hydrocarbons. Hydrocarbon selectivity in the C_5-C_{12} hydrocarbon range is mostly affected by the number of strong acid sites, with the higher concentration of iso-paraffins observed for ZSM-5 zeolite. For longer chain hydrocarbons, the zeolite activity in isomerization and cracking is mainly influenced by the spatial effect such as the size and open character of the zeolite pore structure as well as the location of cobalt species. Large pore zeolites exhibit higher selectivity to long chain iso-paraffins and lower selectivity to C_{20+} hydrocarbons. The selectivity of the long-chain iso-paraffins is also favored by the proximity and close contact between cobalt metallic species and Brønsted acid sites.

6. Acknowledgment

The authors gratefully acknowledge the support of the French National Research Agency (ANR-11-IS09-0003 and ANR-12-BS07-0029). The REALCAT platform is benefiting from a Governmental subvention administrated by the French National Research Agency (ANR) within the frame of the 'Future Investments' program (PIA), with the contractual reference 'ANR-11-EQPX-0037'. The Nord-Pas-de-Calais Region and the FEDER are acknowledged for their financial contribution to the acquisition of the equipment of the platform.

Table 1.

Catalysts characterization

Sample	Si/Al	N_2 adsorption over composite/support				Acidity (Py adsorption)	
		S_{BET}, m^2/g	V_{tot}, cm^3/g	V_{mic}, cm^3/g	Ratio V_{mic} (comp.)/ V_{mic}(zeol)	Brønsted (μmol/g)	Lewis (μmol/g)
Co/SiO_2	-	211	0.85	-	-	0	0
SiO_2	-	307	1.3			0	0
Co/ZSM-5	13	232	0.16	0.1	0.83	507	1427
ZSM-5	13	305	0.19	0.12		1090	240
Co/MOR	8	284	0.21	0.13	0.76	345	275
MOR	8	404	0.21	0.17		921	452
Co/BEA	9	282	0.18	0.07	0.46	88	84
BEA	9	556	0.67	0.15		486	834

Table 2.

Catalytic properties of hybrid and impregnated catalysts (P=2 MPa, $H_2/CO=2$, GHSV=34 L/h·g_{Co}, T=250 °C)

Catalysts	X_{CO}, %	Selectivity, C. %							Ratio (iso/total)	
		CH_4	CO_2	C_2-C_4	C_5-C_{12} norm	C_5-C_{12} olef	C_5-C_{12} iso	C_{12}+	C_5-C_{12}	C_{12}+
Co/SiO_2	37.9	6.1	2.1	7.7	10.0	6.7	0.9	66.5	0.06	0.01
Co/ZSM-5	26.8	11.7	0.5	12.7	5.3	1.2	16.4	52.2	0.7	0.14
Co/SiO_2+ZSM-5	26.4	6.0	0.7	8.7	5.1	1.0	18.0	60.5	0.74	0.08
Co/MOR	40.1	9.2	0.6	10.1	12.1	1.1	6.0	60.9	0.31	0.19
Co/SiO_2+MOR	39.7	6.7	1.7	10.3	6.4	1.4	13.3	60.2	0.6	0.14
Co/BEA	17.5	10.5	0.7	13.6	11.2	0.6	7.6	55.8	0.4	0.33
Co/SiO_2+BEA	54.9	7.4	1.5	9.2	9.5	1.3	6.1	65	0.36	0.16

Figure Legend.

Figure 1. Nitrogen adsorption/desorption isotherms obtained at 77K over the reference Co/SiO_2 and cobalt zeolite catalyst prepared by impregnation.

Figure 2. SEM images of zeolites

Figure 3. TEM images of the Co/ZSM-5, Co/MOR and Co/BEA catalysts

Figure 4. FTIR spectra in the OH region of parent zeolites and cobalt zeolite catalysts

Figure 5. FTIR spectra observed after adsorption of pyridine over parent zeolites and cobalt zeolite catalysts

Figure 6. Desorption of Py from Brønsted acid sites of parent zeolites measured by FTIR with increase of the temperature

Figure 7. IR bands resulting from CO adsorption at room temperature on the reference and composite catalysts (P_{CO}=20 torr)

Figure 8. H_2-TPR profiles for the reference Co/SiO_2 and cobalt zeolite catalysts.

Figure 9. CO conversion as a function of time (P=20 bar, H_2/CO=2, GHSV=34 L/h·g_{Co}, T=250°C) over hybrid and impregnated catalysts

Figure 10. Selectivity to olefins, paraffins and isomers as a function of the chain length over reference, hybrid and impregnated catalysts

Figure 11. Distribution of isomers and paraffins in the liquid products

Figure 12. The ASF chain growth probabilities determined for hydrocarbons over hybrid (a) and composite catalysts (b)

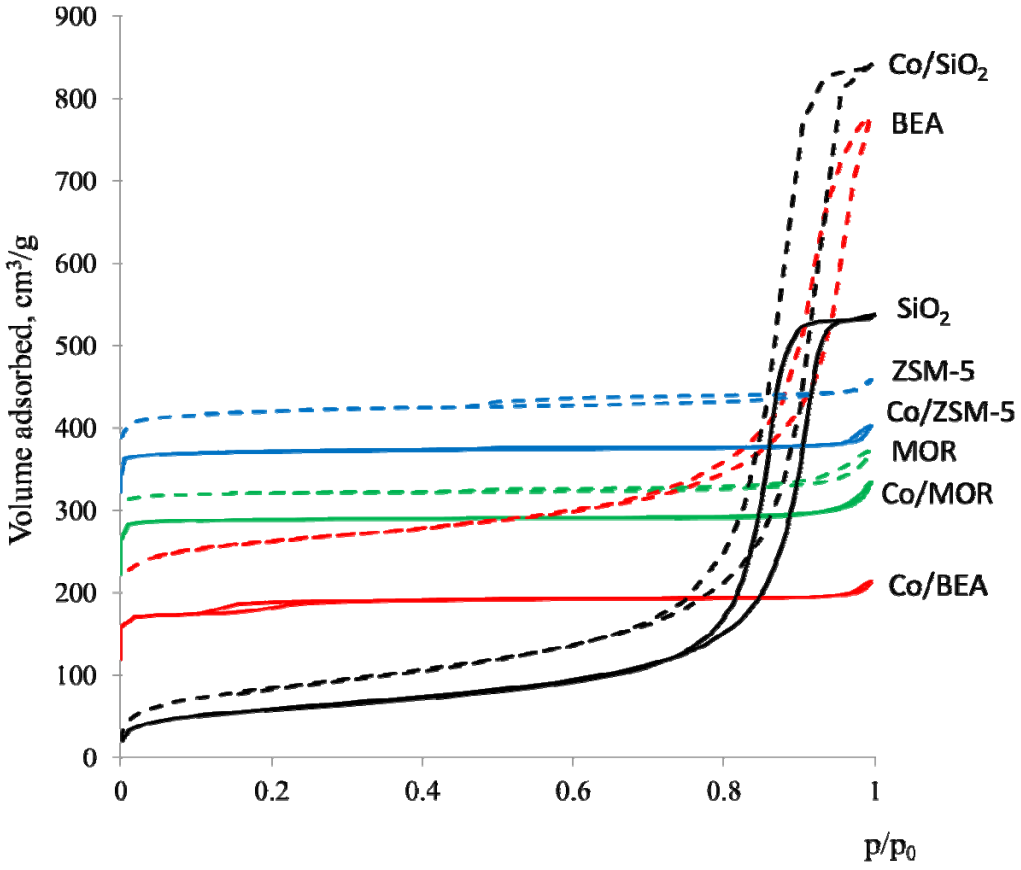
900
800
700
600
500
400
300
200
100
0
0
0.2
0.4
0.6
0.8
1
Volume adsorbed, cm³/g
p/p0
Co/SiO2
BEA
SiO2
ZSM-5
Co/ZSM-5
MOR
Co/MOR
Co/BEA

Figure 1.

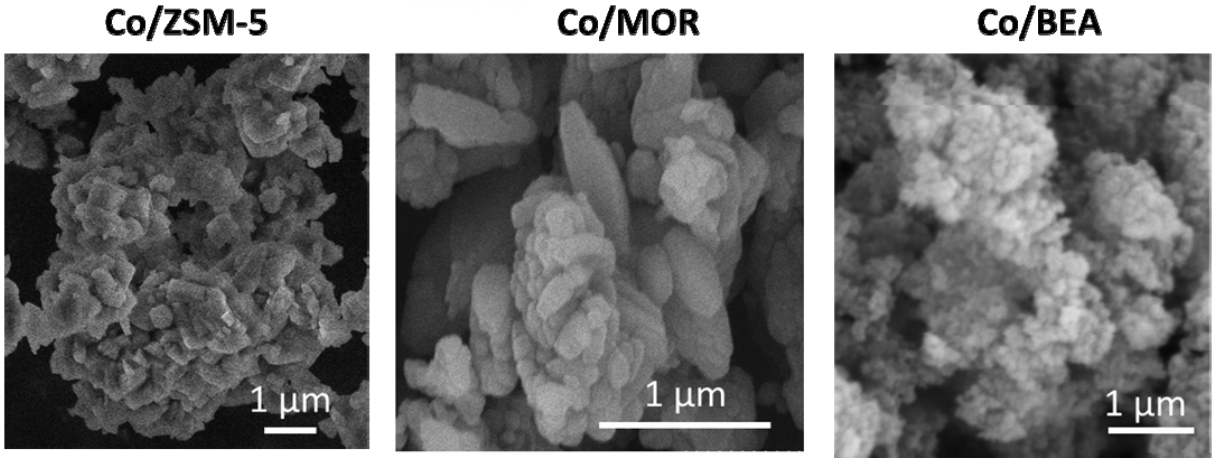

Figure 2.

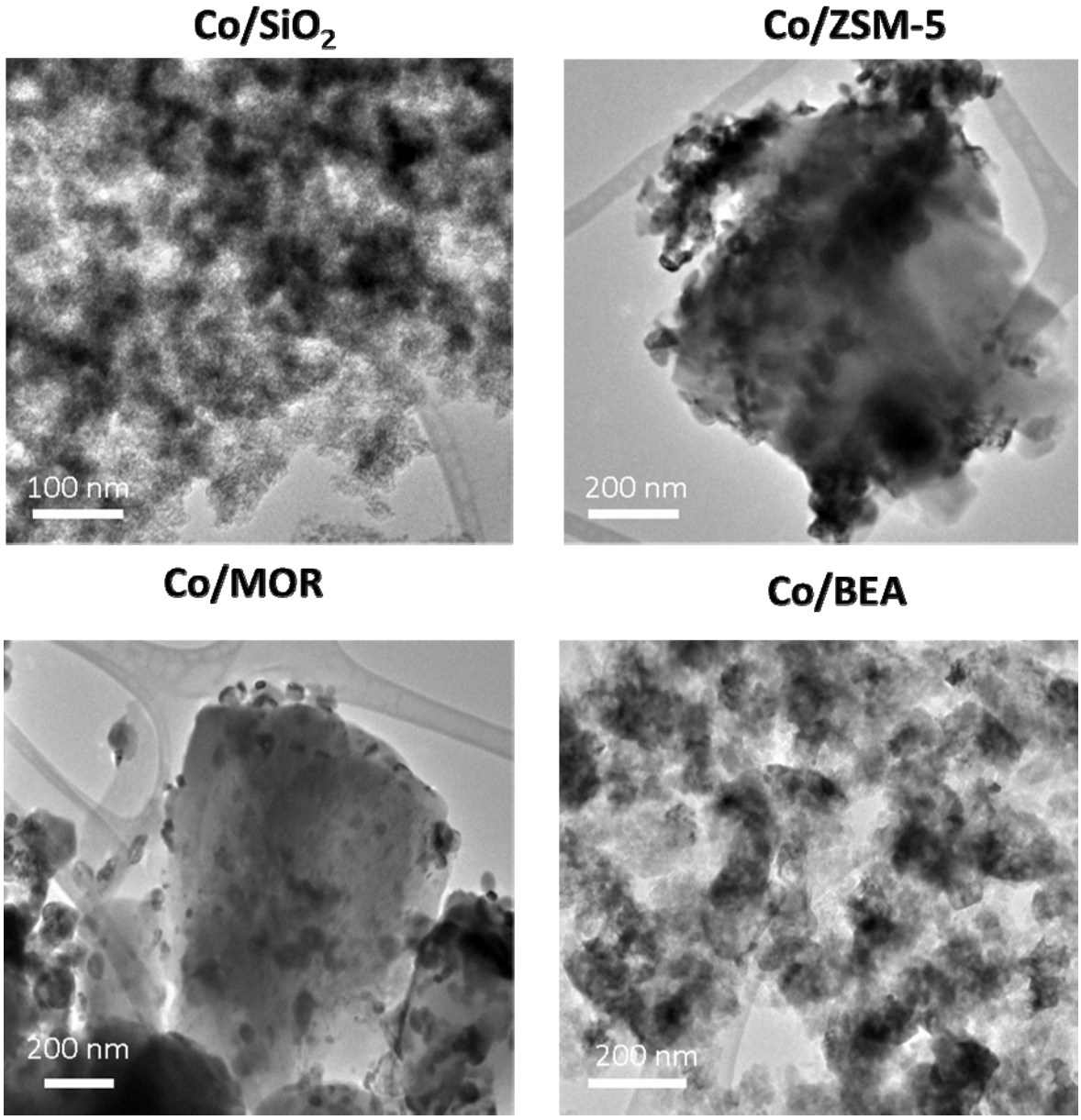

Figure 3.

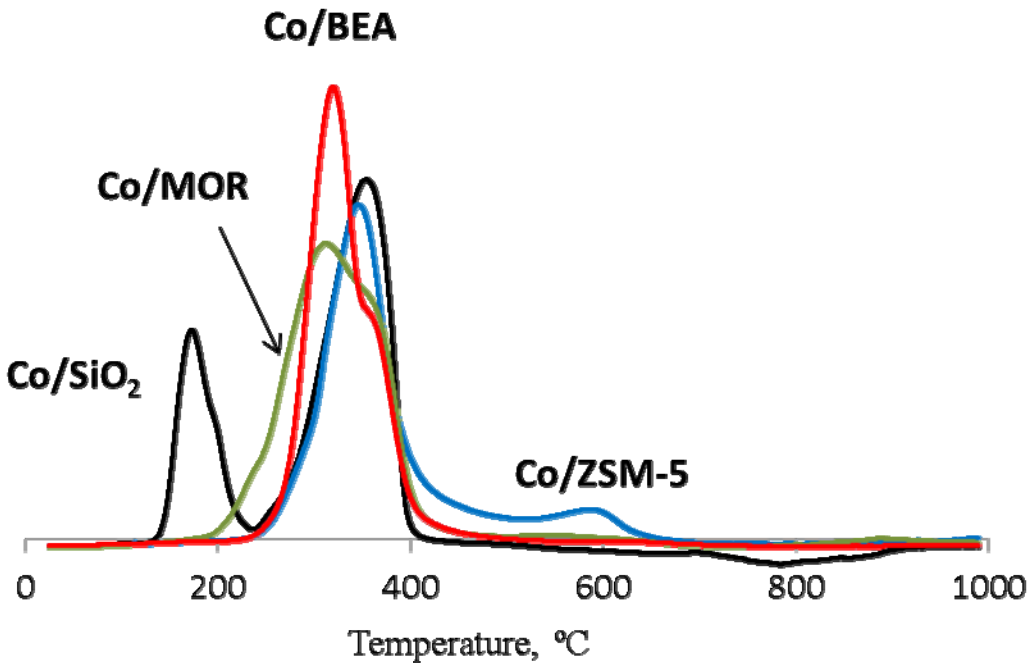
Co/BEA
Co/MOR
Co/SiO2
Co/ZSM-5
0
200
400
600
800
1000
Temperature, ºC

Figure 4.

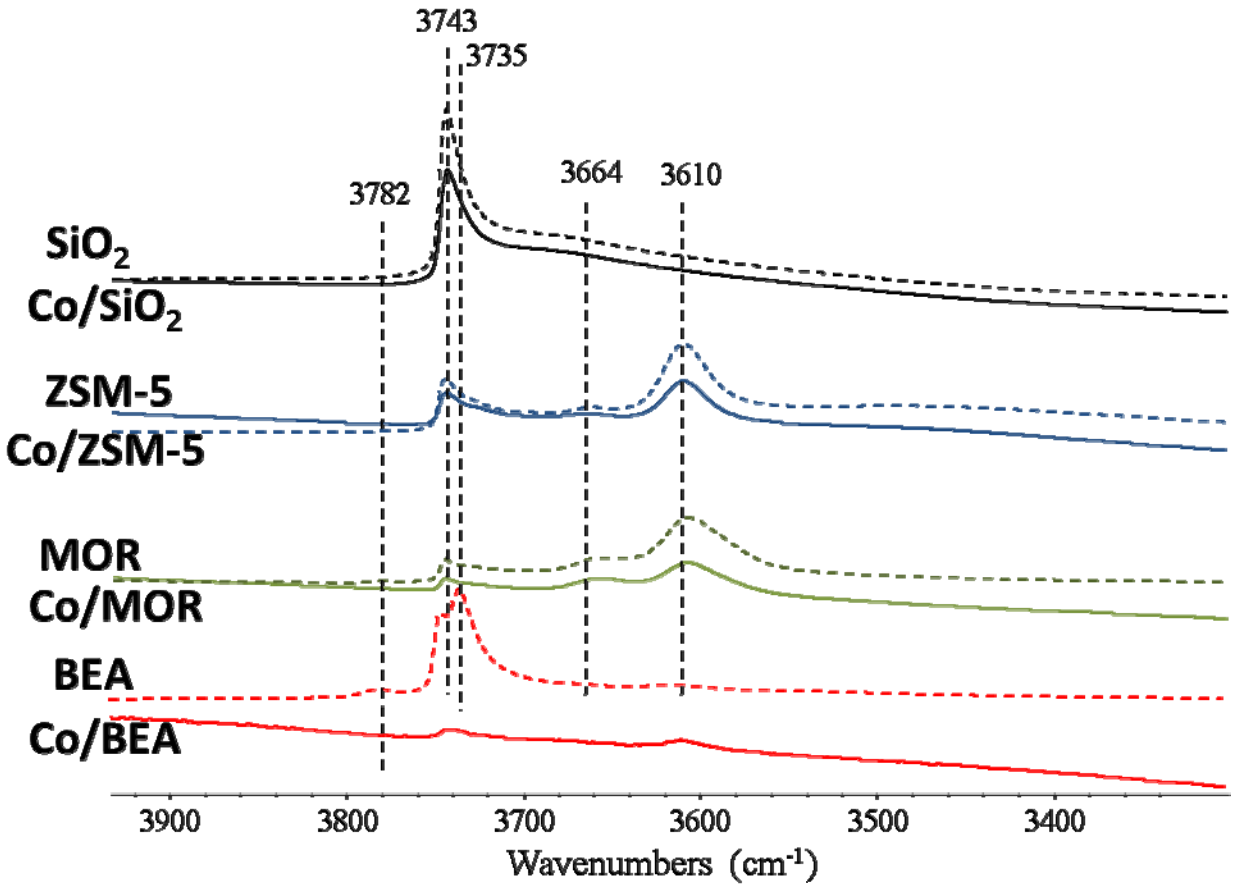
3743
3735
3782
3664
3610
SiO2
Co/SiO2
ZSM-5
Co/ZSM-5
MOR
Co/MOR
BEA
Co/BEA
3900
3800
3700
3600
3500
3400
Wavenumbers (cm-1)

Figure 5.

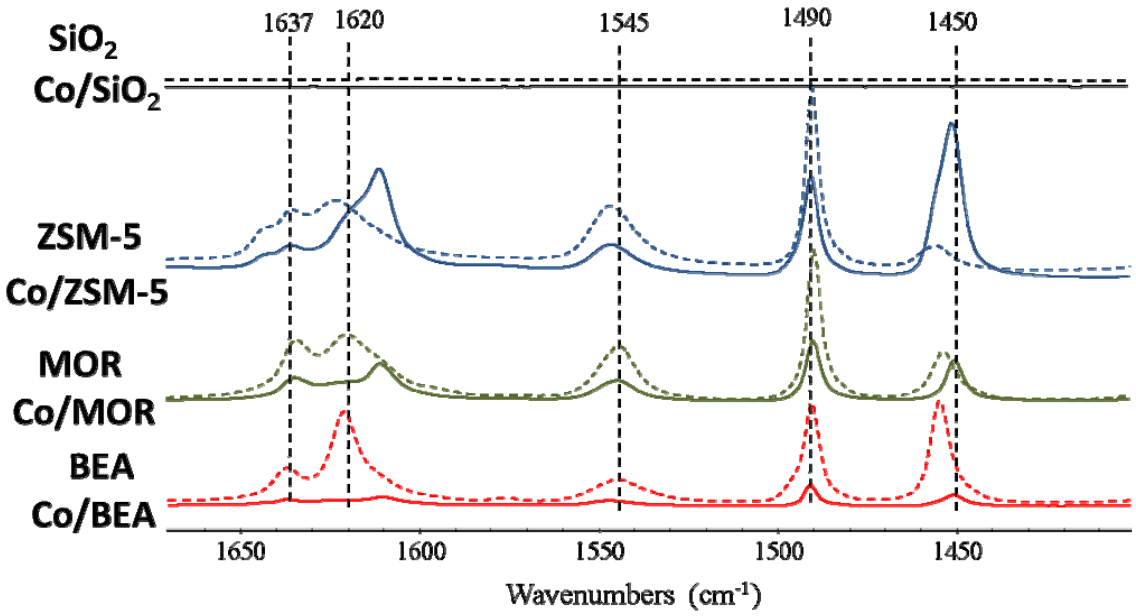
1637
1620
1545
1490
1450
SiO2
Co/SiO2
ZSM-5
Co/ZSM-5
MOR
Co/MOR
BEA
Co/BEA
1650
1600
1550
1500
1450
Wavenumbers (cm-1)

Figure 6.

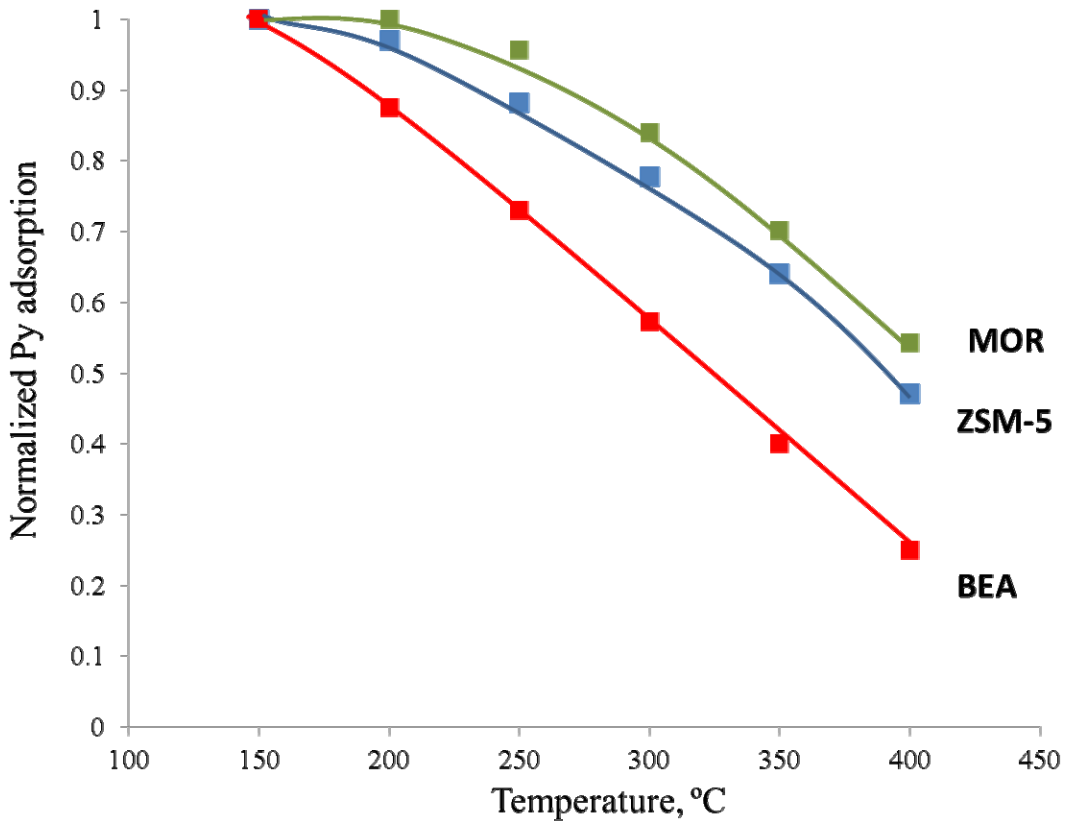
Normalized Py adsorption
1
0.9
0.8
0.7
0.6
0.5
0.4
0.3
0.2
0.1
0
100
150
200
250
300
350
400
450
Temperature, °C
MOR
ZSM-5
BEA

Figure 7.

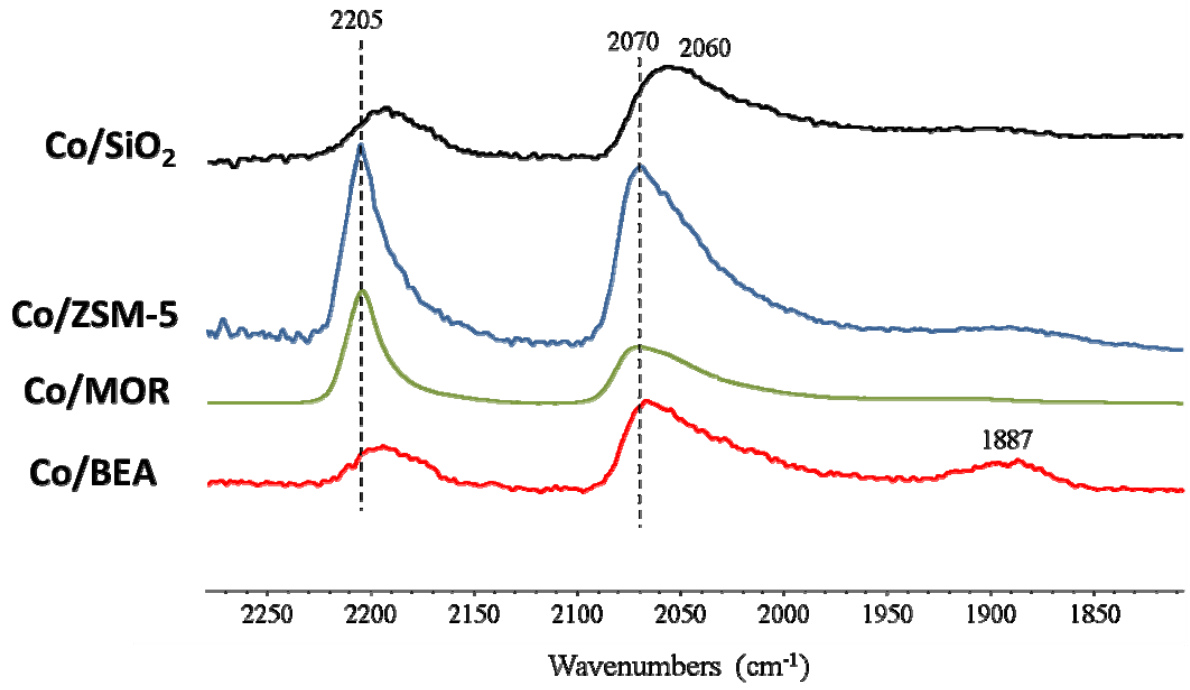
2205
2070
2060
Co/SiO2
Co/ZSM-5
Co/MOR
Co/BEA
1887
2250
2200
2150
2100
2050
2000
1950
1900
1850
Wavenumbers (cm-1)

Figure 8.

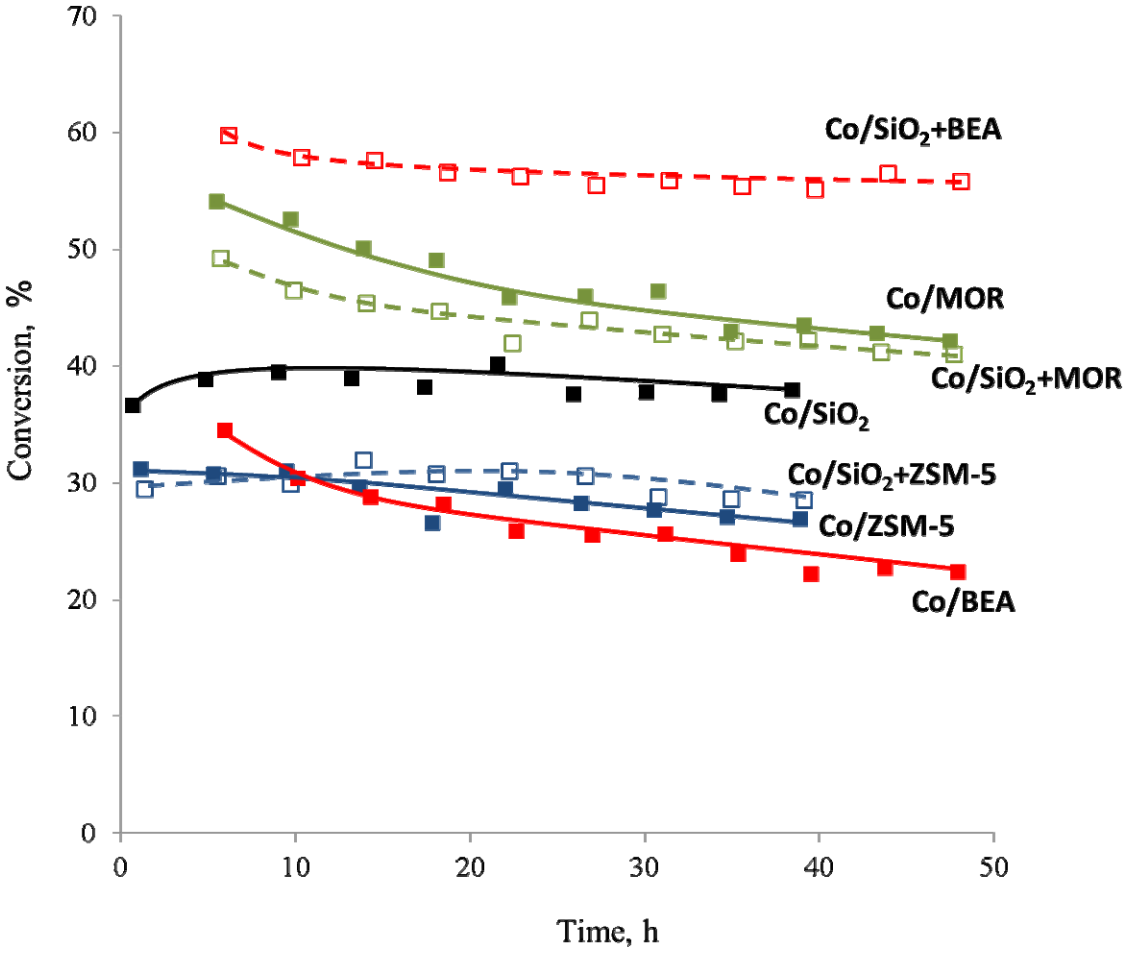
Conversion, %
Time, h
Co/SiO2+BEA
Co/MOR
Co/SiO2+MOR
Co/SiO2
Co/SiO2+ZSM-5
Co/ZSM-5
Co/BEA

Figure 9.

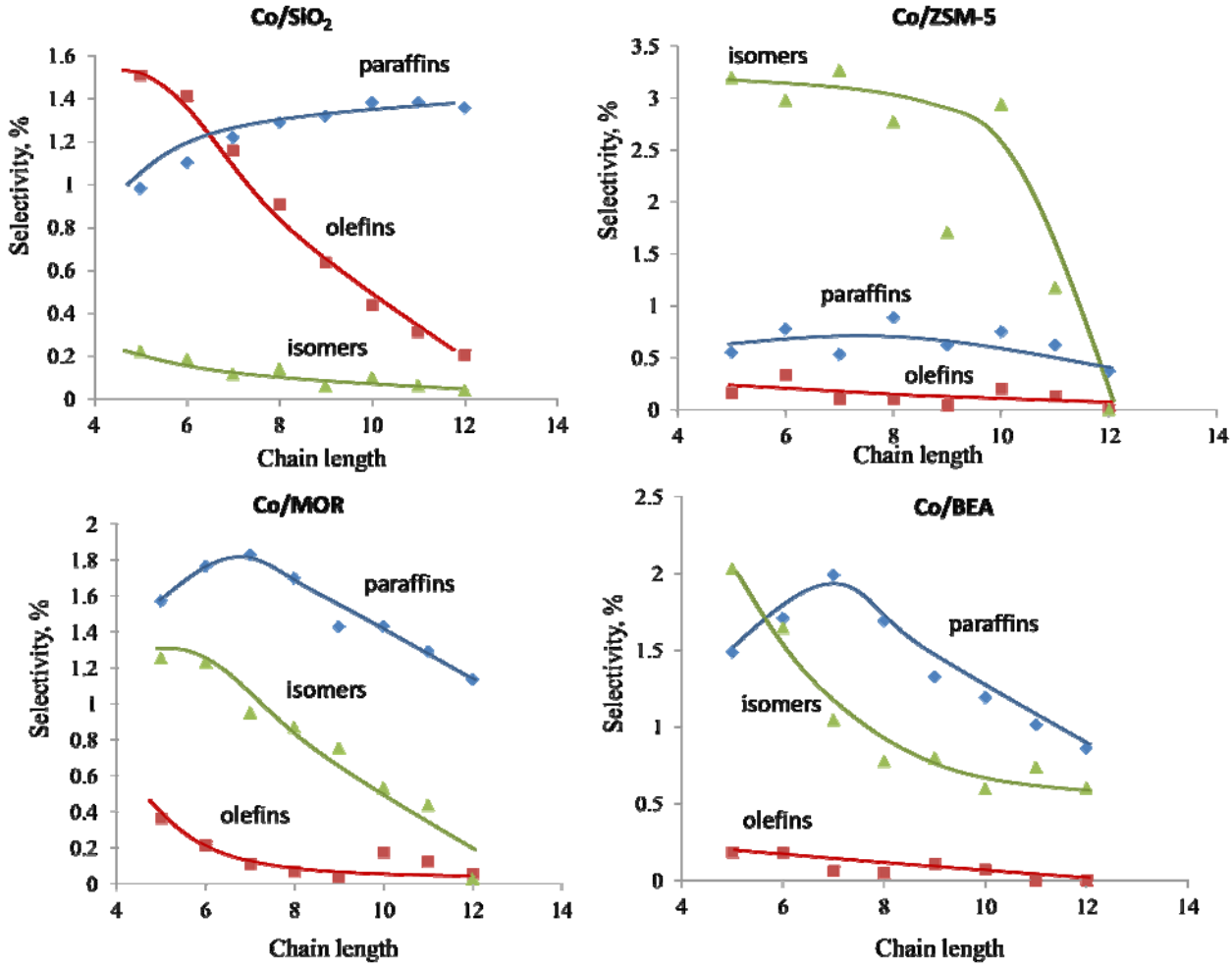
Co/SiO2
paraffins
olefins
isomers
Selectivity, %
Chain length
Co/ZSM-5
isomers
paraffins
olefins
Selectivity, %
Chain length
Co/MOR
paraffins
isomers
olefins
Selectivity, %
Chain length
Co/BEA
paraffins
isomers
olefins
Selectivity, %
Chain length

Figure 10.

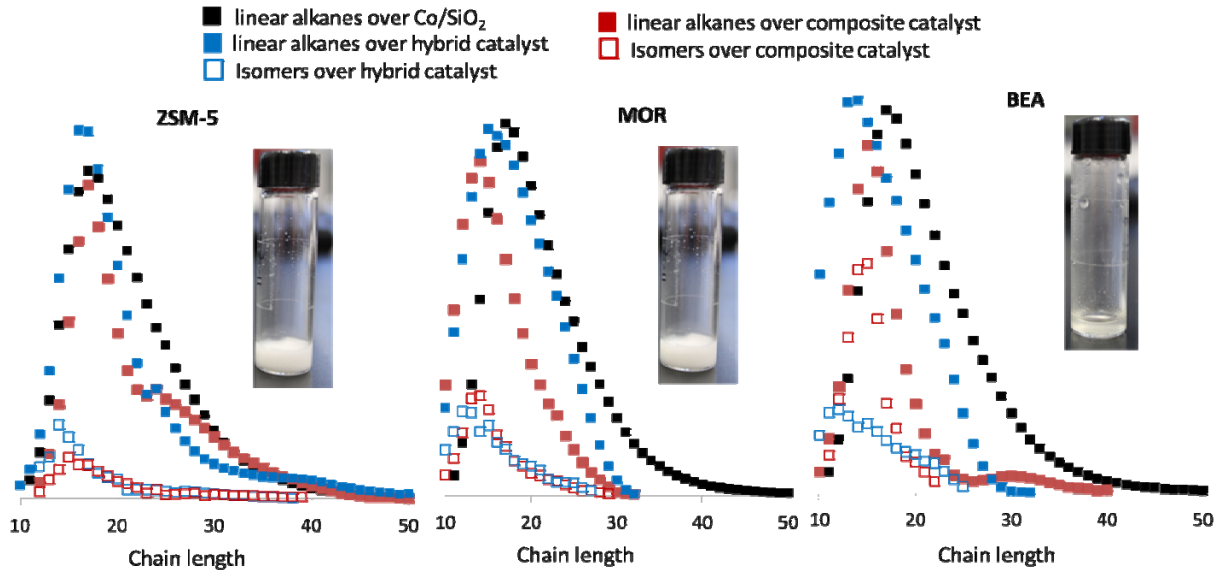
linear alkanes over Co/SiO2
linear alkanes over hybrid catalyst
Isomers over hybrid catalyst
linear alkanes over composite catalyst
Isomers over composite catalyst
ZSM-5
MOR
BEA
10
20
30
40
50
Chain length

Figure 11.

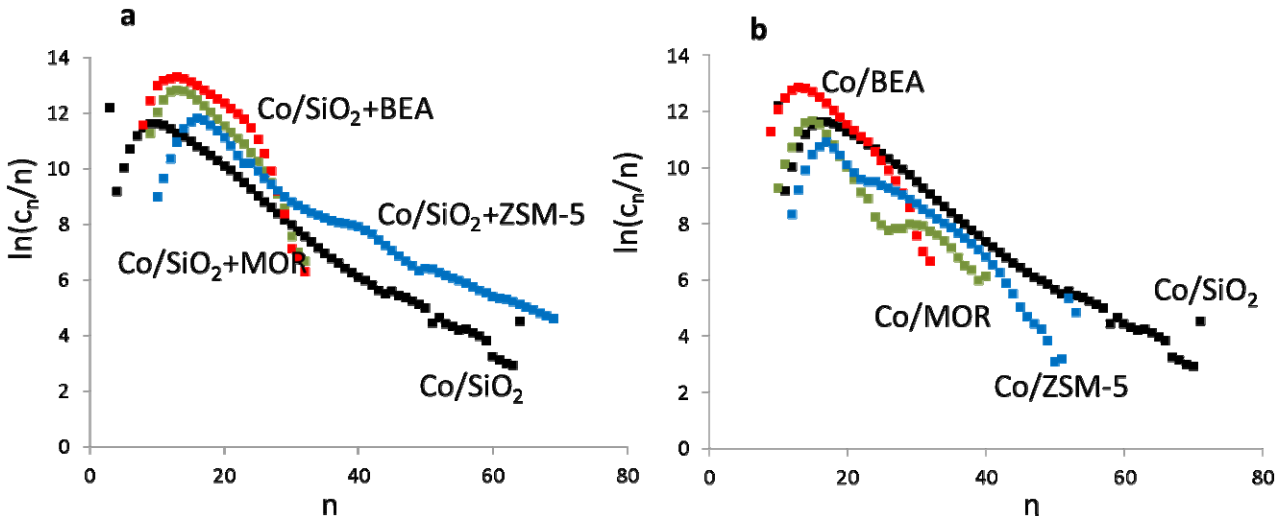
a
b
ln(cn/n)
n
Co/SiO2+BEA
Co/SiO2+ZSM-5
Co/SiO2+MOR
Co/SiO2
Co/BEA
Co/MOR
Co/ZSM-5
0
2
4
6
8
10
12
14
0
20
40
60
80

Figure 12.

Reference

1 B. H. Davis, M. L. Occelli, Advances in Fischer-Tropsch Synthesis, Catalysts, and Catalysis, CRC Press, 2009, p.424.

2 A.Y. Khodakov, W. Chu, P. Fongarland, Chem. Rev. 107 (2007) 1692-1744.

3 Q. Zhang, K. Cheng, J. Kang, W. Deng and Y. Wang, ChemSusChem 7 (2014) 1251-1264.

4 H. Schulz, Catalysis Today, 2014, 228, 113

5 G. Henrici-Olive, S. Olive, Angew. Chem. Int. Ed. 15 (1976) 136-141.

6 Ch.-X. Xiao, Zh.P. Cai, T. Wang, Y. Kou, N. Yan, Angew. Chem. Int. Ed. 47 (2008) 746-749.

7 R. Sethuraman, N.N. Bakhshi, S.P. Katikaneni, R.O. Idem, Fuel Process. Technol. 73 (2001) 197.

8 T.-S. Zhao, J. Chang, Y. Yoneyama, N. Tsubaki, Ind. Eng. Chem. Res. 44 (2005) 769.

9 F.G. Botes, W. Böhringer, Appl. Catal., A Gen. 267 (2004) 217.

10 B. Zeng, B. Hou, L. Jia, J. Wang, C. Chen, D. Li, Y. Sun, Catalysis Science and Technology 3 (2013) 3250-3255

11 G. Yang, C. Xing, W. Hirohama, Y. Jin, C. Zeng, Y. Suehiro, T. Wang, Y. Yoneyama, N. Tsubaki, N. Catal. Today 215 (2013) 29-35

12 X. Li, J. He, M. Meng, Y. Yoneyama, N. Tsubaki, J. Catal. 265 (2009) 26-34

13 R. Xie, D. Li, B.Hou, B., J. Wang, L. Jia, Y. Sun, Catal. Commun.12 (2011) 380-383

14 N. Tsubaki, Y. Yoneyama, K. Michiki, K. Fujimoto, Catal. Commun. 4 (2003) 108.

15 Z.-W. Liu, X. Li, K. Asami, K. Fujimoto, Catal. Commun. 8 (2005) 503.

16 S. Bessell, Appl. Catal. A Gen. 126 (1995) 235.

17 D.J. Koh, J.S. Chung, Y.G. Kim, Ind. Eng. Chem. Res. 34 (1995) 1969.

18 K. Jothimurugesan, S.K. Gangwal, Ind. Eng. Chem. Res. 37 (1998) 1181.

19 A. Martinez, S. Valencia, R. Murciano, H.S. Cerqueira, A.F. Costa, E.F.S.-Aguiar, Appl. Catal A 346 (2008) 117.

20 N. Tsubaki, Y. Yoneyama, K. Michiki, K. Fujimoto, Catal. Commun. 4 (2003) 108.

21 A. Martinez, J. Rollan, M.A. Arribas, HS. Cerqueira, A.F. Costa, E.F. S.-Aguiar, J. Catal. 249 (2007) 162.

22 Z.-W. Liu, X. Li, K. Asami, K. Fujimoto, Catal. Commun. 6 (2005) 503.

23 Z.-W. Liu, X. Li, K. Asami, K. Fujimoto, Fuel Process. Technol. 88 (2007) 165.

24 S. Bessel, Appl. Catal. A Gen 96 (1993) 253.

25 K. Cheng, L. Zhang, J. Kang, X. Peng, Q. Zhang, Y. Wang, Chem. Eur. J. 21 (2015) 1928.

26 S. Sartipi, M. Alberts, M.J. Meijerink, T.C. Keller, J. Perez-Ramirez, J. Gascon, F. Kapteijn, ChemSusChem 6 (2013) 1646.

27 J.H. de Boer, B.C. Lippens, B.G. Linsen, J.C.P. Broekhoff, A. van den Heuvel, Th.V. Osinga, J. Colloid Interface Sci. 21 (1966) 405-414.

28 http://avantium.com/uploads/brochures/avantium-chemicals-flowrence.pdf

29 A. Simon-Masseron, J.P. Marques, J.M. Lopes, F. Ramoa Ribeiro, I.Gener, M. Guisnet, Appl. Catal. A, Gen. 316 (2007) 72.

30 J. Hong, E. Marceau, A.Y. Khodakov, A. Griboval-Constant, C. La Fontaine, V. Briois, Chemistry - A European Journal 2012, 18 (10), pp. 2802-2805.

31 W. Chu, P.A. Chernavskii, L. Gengembre, G.A. Pankina, P. Fongarland and A.Y. Khodakov, J. Catal. 252 (2007) 215.

32 B. Ernst, A. Bensaddik, L. Hilaire, P. Chaumette and A. Kiennemann, Catal.Today 39(1998) 329.

33 C. Resini, T. Montanari, L. Nappi, G. Bagnaco, M. Turco, G. Busca, F. Bregani, N. Notaro, G. Rocchini, J. Catal., 214 (2003), pp. 179–190

34 G. Bagnasco, M. Turco, C. Resini, T. Montanari, M. Bevilacqua, G. Busca, J. Catal., 225 (2004), pp. 536–540

35 X. Wang, H. Chen, W.M.H. Sachtler, Appl. Catal. B, 29 (2001), pp. 47–60

36G. Espinosa, J.M. Domínguez, P. Morales-Pacheco, A. Tobon, M. Aguilar, J. Benítez, Catal. Today 166 (2011) 47.

37 J. Pierez-Pariente, J. Sanz, V. Fornés, A.Corma, J. Catal. 124 (1990) 217.

38 C. Paze , A. Zecchina, S. Spera, A. Cosma, E. Merlo, G. Spano, G. Girotti, Phys. Chem. Chem. Phys. 1 (1999) 2627.

39 J. C. Jansen, E. J. Creyghton, S. L. Njo, H. van Koningsveld, H. van Bekkum, Catal. Today 38 (1997) 205

40 M. Maache, A.Janin, J.C. Lavalley, J.F. Joly, E. Benazzi, Zeolites 13 (1993) 419.

41 F.Lonyi and J.Valyon, Thermochim. Acta, 373 (2001) 53.

42 M. Guisnet, P. Ayrault, C. Coutanceau, M.F. Alvarez, J. Datka, J. Chem. Soc. Faraday Trans. 93 (1997) 1661.

43 K. Chakarova, K. Hadjiivanov, Micropor. Mesopor. Mater. 123 (2009) 123.

44 A. Y. Khodakov, J. Lynch, D. Bazin, B. Rebours, N. Zanier, B. Moisson and P. Chaumette, J. Catal. 168 (1997) 16-25.

45 M. Jiang, N. Koizumi, T. Ozaki, M. Yamada, Appl. Catal. A 209 (2001) 59.

46 J. Ansorge, H. Foerster, J. Catal. 68 (1981) 182

47 S. Sartipi, K. Parashar, M.J. Valero-Romero, V.P. Santos, B. van der Linden, M. Makkee, F. Kapteijn, J. Gascon, J. Catal. 305 (2013) 179.

48 E. Iglesia, S.C. Reyes, R.J. Madon and S.L. Soled, Adv. Catal. 39 (1993) 221.

49 E. Iglesia, E. Appl. Catal. A 161 (1997) 59.

50 V.G. Komvokisa, S. Karakouliaa, E.F. Iliopouloua, M.C. Papapetroua, I.A. Vasalosa, A.A. Lappasa, K.S. Triantafyllidis, Catalysis Today 196 (2012) 42.